

APPROXIMATION OF INTEGRAL FRACTIONAL LAPLACIAN AND FRACTIONAL PDES VIA SINC-BASIS

HARBIR ANTIL, PATRICK DONDL, AND LUDWIG STRIET

ABSTRACT. Fueled by many applications in random processes, imaging science, geophysics, etc., fractional Laplacians have recently received significant attention. The key driving force behind the success of this operator is its ability to capture non-local effects while enforcing less smoothness on functions. In this paper, we introduce a spectral method to approximate this operator employing a sinc basis. Using our scheme, the evaluation of the operator and its application onto a vector has complexity of $\mathcal{O}(N \log(N))$ where N is the number of unknowns. Thus, using iterative methods such as CG, we provide an efficient strategy to solve fractional partial differential equations with exterior Dirichlet conditions on arbitrary Lipschitz domains. Our implementation works in both $2d$ and $3d$. We also recover the FEM rates of convergence on benchmark problems. We further illustrate the efficiency of our approach by applying it to fractional Allen-Cahn and image denoising problems.

CONTENTS

1. Introduction	2
2. The sinc-Fractional Laplacian	4
2.1. sinc-Interpolation	4
2.2. The discrete operator	6
3. Numerical Methods and Error Estimates	7
3.1. Computation of the periodic fractional Laplacian	8
3.2. Equivalence of the scaled periodic fractional Laplacian and the sinc-fractional Laplacian	9
3.3. Setting up the convolution kernel	10
3.4. Solving the Dirichlet problem	13
3.5. Summary of algorithms and computational complexity	14
4. Numerical Experiments	15
4.1. Quadrature rules for the convolution kernel	16
4.2. Function with constant fractional Laplacian on the unit sphere	17

LS gratefully acknowledges a doctoral scholarship from the Friedrich-Ebert-Stiftung. HA is partially supported by NSF grants DMS-1818772, DMS-1913004, the Air Force Office of Scientific Research (AFOSR) under Award NO: FA9550-19-1-0036, and Department of Navy, Naval PostGraduate School under Award NO: N00244-20-1-0005.

4.3. Fractional Allen-Cahn equation	18
4.4. Image denoising	21
5. Conclusion and Future Work	23
References	24

TABLE 1. Symbols and notations used throughout the paper.

Symbol	Description
\mathcal{I}_N^d	Index set $\{0, \dots, N-1\}^d$ where $N, d \in \mathbb{N}$
\mathcal{I}_N^{id}	Index set $\{-N/2, \dots, N/2-1\}^d$ where $N, d \in \mathbb{N}$
\mathcal{F}	Fourier transformation
\mathcal{F}^{-1}	Inverse Fourier transformation
DFT	Discrete Fourier transformation
IDFT	Inverse discrete Fourier transformation
$(-\Delta)^s$	Integral fractional Laplacian
$(-\Delta)^s$	Periodic fractional Laplacian
$(-\Delta)_N^s$	N -point sinc-fractional Laplacian
$(-\Delta)_N^s$	N -point discrete periodic fractional Laplacian
$(-\Delta)_{S,N}^s$	N -point scaled discrete periodic fractional Laplacian

1. INTRODUCTION

This article is concerned with the numerical treatment of equations of the form

$$\begin{aligned} (-\Delta)^s u &= f && \text{in } \Omega \\ u &= 0 && \text{in } \mathbb{R}^d \setminus \Omega, \end{aligned} \tag{1.1}$$

on an open bounded domain $\Omega \subset \mathbb{R}^d$ with Lipschitz boundary $\partial\Omega$. Furthermore, we consider applications to phase field models and imaging science.

A standard way to define the fractional Laplacian is via a principle value integral on functions in the Schwartz space $\mathcal{S}(\mathbb{R}^d)$ of rapidly decaying functions.

Definition 1.1. Let $u \in \mathcal{S}(\mathbb{R}^d)$ and $s \in (0, 1)$. The operator $(-\Delta)^s$ is defined as

$$(-\Delta)^s u(x) = C(d, s) P.V. \int_{\mathbb{R}^d} \frac{u(x) - u(y)}{|x - y|^{d+2s}} dy \tag{1.2}$$

where

$$C(d, s) = \frac{s 2^{2s} \Gamma(s + d/2)}{\pi^{d/2} \Gamma(1 - s)} \tag{1.3}$$

is a normalization constant.

This definition clearly shows the non-local character of the operator $(-\Delta)^s$. In order to evaluate $(-\Delta)^s u(x)$ at a single point $x \in \mathbb{R}^d$, one has to evaluate the singular integral over the full space \mathbb{R}^d . Furthermore, this fractional Laplacian only makes sense for functions which are defined on all of \mathbb{R}^d .

For the remainder of this paper, we will refer to problems of the form (1.1) as the Dirichlet problem for the fractional Laplacian, or – more explicitly – as the fractional Poisson problem with Dirichlet exterior conditions. The fractional Laplacian of a function u with support in $\Omega \subset \mathbb{R}^d$, Ω bounded, or, equivalently, of a function $u: \Omega \rightarrow \mathbb{R}$ which is extended by zero outside Ω will be denoted as the Dirichlet fractional Laplacian. We remark that other options to give meaning to fractional operators applied to functions defined on bounded domains exist (for an overview, see [25]), but here, we will be concerned with the Dirichlet problem as described above.

A common equivalent way to define the fractional Laplacian is via a Fourier multiplier [19].

Theorem 1.1. *Let $s \in (0, 1)$ and let $(-\Delta)^s : \mathcal{S}(\mathbb{R}^d) \rightarrow L^2(\mathbb{R}^d)$ the fractional Laplacian of Definition 1.1. Then, for $u \in \mathcal{S}$,*

$$(-\Delta)^s u = \mathcal{F}^{-1} (|\omega|^{2s} (\mathcal{F} u)). \quad (1.4)$$

In principle, (1.4) gives a direct method to solve (1.1) via the Fourier transformation. This is, of course, numerically intractable as it is not possible to perform a discrete Fourier transformation (DFT) on an infinite domain. On the other hand, if one truncates the domain on which the Fourier transformation is performed, one instead obtains the fractional Laplacian of a function u that was periodically extended outside the truncation. We note that this is a different operator than the Dirichlet fractional Laplacian that we will call *periodic fractional Laplacian*, denoted $(\widetilde{-\Delta})^s$.

Fractional partial differential equations (PDEs) of type (1.1) have recently received a significant amount of attention. The interest in fractional operators of type $(-\Delta)^s$ with $s \in (0, 1)$ stems from two facts: (i) these operators impose less smoothness (cf. the classical case $s = 1$); (ii) even more importantly, these operators easily enable nonlocal interaction, recall that the classical derivatives lead to local operators.

The fractional Laplacian has been used as a regularizer in imaging [5, 6]. Additionally, it can be derived using the so called long jump random walk [35]. Finally, the fractional Helmholtz equation has been recently derived in [36] using the first principle arguments in conjunction with a constitutive relation. We emphasize that the fractional Laplacian in [36] is of the so-called spectral type. From an optimal control point of view, fractional operators provide a great deal of flexibility, in fact, since the condition $u = 0$ is imposed in the exterior of the domain $(\mathbb{R}^d \setminus \Omega)$, therefore it has been possible to introduce a new type of optimal control (called Exterior Control) using fractional PDEs [7].

It has been noted in [14] that – in \mathbb{R}^d – the definitions (1.2) and (1.4) are further equivalent to the so called extension problem. However, this is also no longer the case in case of bounded domains. Nevertheless, it is still possible to define an extension problem which is equivalent to the so-called spectral fractional Laplacian [34]. Using such an extension, efficient finite element based numerical methods have been proposed in [29, 27]. For completeness, we also refer to [8] for an extension problem where the fractional exponent s is a function of the spatial variable $x \in \Omega$.

On the other hand, the numerical methods for problems of the type (1.1) present even more challenges, as one needs to resolve the singular integrals. The first work that rigorously tackles numerics for (1.1) using finite element method is by Acosta and Borthagaray [2], see also [3].

However, the implementations in these works have been limited to $d = 2$ dimensions. We also refer to another finite element approach of Bonito, Lei, and Pasciak [11], which also works in $d = 3$ [10].

In contrast, we provide a spectral method to approximate the Dirichlet fractional Laplacian (1.2) where we attempt to combine fast Fourier transform (FFT) efficiency with the ability to treat exterior value problems as in (1.1). As we shall illustrate with numerical examples, this approach directly applies to the case when $d = 3$, and extension to even higher dimensions is possible given efficient FFT implementations. Using our method, the application of the fractional operator has the same numerical complexity as a Fourier transform. To solve the Dirichlet problem (1.1) we then use this operator, restricted to Ω , within a conjugate gradient algorithm.

Related strategies have been suggested recently by other authors. Duo and Zhang introduced a finite difference scheme to efficiently solve equations involving the fractional Laplace operator [20]. Their method relies on a finite difference approximation of the operator and the fact that this can be expressed as a matrix consisting of blocks of symmetric Toeplitz-Matrices which can be applied efficiently using discrete Fourier transformation based methods. Given this operator, they solve fractional PDEs using iterative methods. Minden and Ying introduced a method to discretize the integral operator (1.2) which also leads to a Toeplitz-Matrix. Along with a preconditioner, they also use the conjugate gradient method to solve the arising systems for the fractional Dirichlet problem and fractional diffusion equations [28]. Another example for a spectral method was provided recently by Xu and Darve. They use eigenfunctions and eigenvalues w.r.t a specific weight of the Dirichlet fractional Laplacian to solve the fractional Dirichlet problem on the unit ball [37].

A more general, unified framework for finite difference schemes to evaluate Fractional Laplacians for $d = 1$ is presented by Huang and Oberman in [24]. In particular, they presented a finite difference scheme based on sinc-interpolation and show an equivalence to a Fourier scheme on an infinite interval. We extend those results to multiple dimensions and present numerical schemes to calculate the resulting integrals.

The article is organized as follows. In section 2 we briefly discuss some properties of the sinc-interpolation used in the present work as well as a discrete version of the fractional Laplacian based on this interpolation. The numerical methods to efficiently evaluate fractional Laplacians, as well as some equivalences between scaled periodic and our discretized operators, are presented in section 3, with the algorithms listed in section 3.5. Section 4 is devoted to validation of our theoretical results using various numerical examples in both $d = 2$ and $d = 3$. The expected theoretical rates from the convergence from the finite element method of [2] are obtained in both cases. We conclude the paper by successfully applying the proposed scheme to the fractional Allen-Cahn equation and image denoising problems.

2. THE SINC-FRACTIONAL LAPLACIAN

In this section, we define our discrete approximation of the Dirichlet fractional Laplacian. First, in section 2.1, we introduce an appropriate discretization method for functions with bounded support. Following this, we use a discrete convolution to define our operator in section 2.

2.1. sinc-Interpolation. It is a well-known fact that, for example, smooth functions with compact support on \mathbb{R} can be well approximated by a weighted sum of scaled and shifted sinc-functions.

The sinc-function is defined as

$$\text{sinc}(x) = \frac{\sin(\pi x)}{\pi x}. \quad (2.1)$$

Two different approaches of approximating functions with sinc-functions are found in the literature. The first approach is to consider the sinc-function as a wavelet scaling function and then to approximate in the sense of wavelets which leads to the so called Shannon-wavelets. A good overview on such techniques can be found in [16]. They have also been used to approximate fractional derivatives as shown in [17, 18].

The second approach, which we will pursue here, is to approximate a function $u : \mathbb{R} \rightarrow \mathbb{R}$ by

$$u(x) \approx \sum_{k=-\infty}^{\infty} u(kh) \text{sinc}\left(\frac{x - kh}{h}\right). \quad (2.2)$$

The sum on the right hand side (if it converges) is called *Whittaker Cardinal Function*, see, e.g., [26] for more details. This approximation is rather precise [33] and has found numerous applications, e.g., for solving ordinary differential equations, partial differential equations and integral equations [32, 33], but also for approximating integrals arising in fractional calculus [9]. Furthermore, this is the method chosen in [24] to derive the weights for a finite difference scheme to compute fractional Laplacians in one dimension.

In this work, we will use approximations similar to (2.2), extended to multiple dimensions. For $x \in \mathbb{R}$, we set

$$\varphi(x) = \text{sinc}(x) \quad (2.3)$$

as the reference basis function and define its scaled and shifted version $\varphi_k^N : \mathbb{R}^d \rightarrow \mathbb{R}$ for $k = (k_1, \dots, k_d)^T \in \mathbb{Z}^d$ by a tensor product

$$\varphi_k^N(x) = \prod_{j=1}^d \varphi(Nx_j - k_j), \quad x = (x_1, \dots, x_d)^T \in \mathbb{R}^d \quad (2.4)$$

where \mathbb{Z}^d is the d -dimensional integer lattice. For $u : \mathbb{R}^d \rightarrow \mathbb{R}$, we obtain the sinc approximation

$$u_N(x) = \sum_{k \in \mathbb{Z}^d} u_k \varphi_k^N(x) \quad (2.5)$$

where

$$u_k = u(x_k), \quad x_k = k/N. \quad (2.6)$$

Since we are interested in computing the Dirichlet fractional Laplacian, our functions have compact support, which we from now on assume to be contained in the unit cube $[0, 1]^d$ (the generalization to other, larger domains is trivial; our assumption is merely for notational convenience). We therefore may truncate the series to

$$u_N(x) = \sum_{k_1=0}^{N-1} \cdots \sum_{k_d=0}^{N-1} u_k \varphi_k^N(x) \quad (2.7)$$

$$= \sum_{k \in \mathcal{I}_N^d} u_k \varphi_k^N(x), \quad (2.8)$$

where, if $\mathcal{I}_N := \{0, \dots, N-1\}$, then $\mathcal{I}_N^d \subset \mathbb{Z}^d$ indicates its d -fold Cartesian product. Later in this work, we will also use the set $\mathcal{I}'_N = \{-N/2, \dots, N/2-1\}$ and its Cartesian product respectively.

It is a well-known fact that the basis function φ can be obtained as the inverse Fourier transform of the indicator function of a square, i.e., for $D = [-\pi; \pi]^d$ we have

$$(\mathcal{F}^{-1}\chi_D(\omega))(x) = (2\pi)^d\varphi(x)$$

where

$$\chi_D(x) = \begin{cases} 1 & \text{if } x \in D \\ 0 & \text{otherwise.} \end{cases}$$

Similarly, $\varphi_k^N(x)$ can be obtained as

$$\begin{aligned} \varphi_k^N(x) &= \varphi(Nx - k) \\ &= \mathcal{F}^{-1} \left(\underbrace{(2\pi N)^{-d}\chi_{D_N}(\omega)e^{-i\omega k/N}}_{=\mathcal{F}\varphi_k^N(\omega)} \right)(x) \end{aligned}$$

where $D_N = [-N\pi; N\pi]^d \subset \mathbb{R}^d$.

2.2. The discrete operator. Given a function u with $\text{supp } u \subset [0; 1]^d \rightarrow \mathbb{R}$, we want to apply the Dirichlet Fractional Laplace operator $(-\Delta)^s$ of equation (1.4) to its sinc-approximation u_N . We shall write

$$(-\Delta)_N^s u := (-\Delta)^s u_N$$

and call the operator $(-\Delta)_N^s$ the *sinc-fractional Laplacian*. We are restricted to grid points, so let $x_\kappa = \kappa/N$, $\kappa \in \mathcal{I}_N^d$. As \mathcal{I}_N^d is finite and $(-\Delta)^s$ is linear, we obtain

$$\begin{aligned} (-\Delta)^s u_N(x_\kappa) &= (-\Delta)^s \left(\sum_{k \in \mathcal{I}_N^d} u_k \varphi_k^N(x_\kappa) \right) \\ &= \sum_{k \in \mathcal{I}_N^d} u_k \underbrace{((-\Delta)^s \varphi_k^N)(x_\kappa)}_{=:\Phi^N(\kappa-k)} \\ &= \sum_{k \in \mathcal{I}_N^d} u_k \Phi^N(\kappa - k). \end{aligned} \tag{2.9}$$

where we have defined $\Phi^N(\kappa - k) = (-\Delta)^s \varphi_k^N(x_\kappa)$ for $k, \kappa \in \mathcal{I}_N^d$. In the remainder of this paper, we will occasionally use the notation $\Phi_K^N = \Phi^N(\kappa - k)$, with $K = \kappa - k$ when it is clear from the context. Notice that (2.9) denotes a discrete convolution. The computation of this convolution is the application of the sinc-fractional Laplacian.

In other words, we obtain the sinc-fractional Laplacian $(-\Delta)^s u_N(x_\kappa)$ for any grid point x_κ as the discrete convolution of $\mathbf{u} = (u_k)_{k \in \mathcal{I}_N^d}$ and Φ^N . Such a convolution can be implemented efficiently using the FFT algorithm once $\Phi^N(\kappa - k)$ is known for all $k, \kappa \in \mathcal{I}_N^d$. More precisely, the *circular* discrete convolution of two vectors $\mathbf{x}, \mathbf{y} \in \mathbb{R}^{N^d}$ can be calculated as

$$(\mathbf{x} *_d \mathbf{y})(k) := \sum_{\kappa \in \mathcal{I}_N^d} \bar{\mathbf{x}}(\kappa) \cdot \bar{\mathbf{y}}(k - \kappa) \tag{2.10}$$

$$= \text{IDFT} \{ (\text{DFT } \mathbf{x}) \circ (\text{DFT } \mathbf{y}) \}(k) \tag{2.11}$$

where \circ denotes the component-wise product of vectors, and DFT and IDFT denote the discrete Fourier transformation and the inverse discrete Fourier transformation, respectively. By circular we

mean that negative components of indices $\kappa - k$ are mapped circularly to their positive counterparts, in formulas

$$\bar{\mathbf{x}}(K) = \begin{cases} \mathbf{x}(K) & \text{if } K \geq 0 \\ \mathbf{x}(K + N) & \text{if } K < 0. \end{cases}$$

While the evaluation of (2.10) is of complexity $\mathcal{O}((N^d)^2)$, if evaluated for each k , the simultaneous evaluation of (2.11) for all k can be implemented in $\mathcal{O}(N^d \log(N^d))$ time.

For our application, we do not actually want to apply the circular convolution, but the convolution where we extend by zero instead of periodically. As we still want to use the FFT-based algorithm to evaluate (2.9) because of its computational efficiency, we set

$$\bar{u}_k = \begin{cases} u_k & \text{if } k \geq 0 \\ 0 & \text{otherwise} \end{cases}$$

where the expression $k \geq 0$ is meant component-wise. Then, we have that

$$(-\Delta)^s u_N(x_\kappa) = (\bar{u} *_d \Phi^N)(\kappa)$$

which we implement using a FFT of size $(2N)^d$. Further details on the implementation and pseudocode can be found in section 3.5.

We have shown that we can obtain the basis function $\varphi(\cdot)$ as the inverse Fourier transformation of the indicator function of a square in \mathbb{R}^d . This can in principle be used to obtain the integral fractional Laplacian $((-\Delta)^s \varphi)$ of the basis functions, since for $x \in \mathbb{R}^d$, we have

$$\begin{aligned} ((-\Delta)^s \varphi)(x) &= \mathcal{F}^{-1}(|\omega|^{2s}(\mathcal{F} \varphi)) \\ &= (2\pi)^{-d} \int_D |\omega|^{2s} e^{i\omega \cdot x} d\omega, \end{aligned} \tag{2.12}$$

and

$$\begin{aligned} \Phi^N(\kappa - k) &= (2\pi N)^{-d} \int_{D_N} |\omega|^{2s} e^{i\omega \cdot (x_\kappa - k/N)} d\omega \\ &= (2\pi)^{-d} N^{2s} \int_D |\omega|^{2s} e^{i\omega \cdot (\kappa - k)} d\omega \\ &= N^{2s} ((-\Delta)^s \varphi)(\kappa - k). \end{aligned} \tag{2.13}$$

However, using this equality directly is impractical as we would have to evaluate the oscillating integral for each multi-index k . For the one dimensional case, it is possible to circumvent this issue through the use of the confluent hypergeometric function [24], but for $d > 1$ a numerical solution must be found.

Clearly, calculating Φ^N itself is not necessary in order to implement (2.9) as we only need the discrete Fourier transformation $\hat{\Phi}^N$ of Φ^N . In section 3.3 we show how $\hat{\Phi}^N$ can be obtained efficiently.

3. NUMERICAL METHODS AND ERROR ESTIMATES

The goal of this section is to introduce our numerical methods. We begin with section 3.1 where we discuss the computation of fractional Laplacians using simple Fourier methods as mentioned in the introduction. In section 3.2, we show that the sinc-fractional Laplacian applied to a function

with support in $[0, 1]^d$, as defined in (2.9), can be seen as a limit $S \rightarrow \infty$ of fractional Laplacians obtained by standard Fourier transforms of the function periodically extended outside $[0, S]^d$.

We then describe, in section 3.3, our numerical quadrature method used to compute $\hat{\Phi}$. The solution strategy to the Dirichlet exterior value problem (1.1) is discussed in section 3.4. Note Table 1 where an overview on our notation is provided.

3.1. Computation of the periodic fractional Laplacian. To experimentally test that our discrete approximation (2.9) indeed approaches the Dirichlet fractional Laplacian, we can compare it to the periodic fractional Laplacian which is calculated by extending u periodically outside of a truncation domain, instead of extending u by 0.

For periodic functions, the periodic fractional Laplacian and the integral fractional Laplacian are equal [1]. If the Dirichlet fractional Laplacian is approximated with the periodic fractional Laplacian on a finite domain, an error is introduced due to the implicit periodization of the function. This effect, however, is reduced if the function is scaled with a factor $S > 1$ before the application of the periodic fractional Laplacian and rescaled to the original domain afterwards. Heuristically, this occurs because the additional support introduced by the periodic continuation becomes shifted further away from the original support. The error is then on the order of $S^{-(d+2s)}$. This estimate is summarized in the following Lemma. The main motivation for this Lemma is the fact that in the next section we shall establish an equivalence between the scaled periodic fractional Laplacian and the sinc-fractional Laplacian, see Theorems 3.1 and 3.2

Lemma 3.1. *Let $\text{supp } u = \Omega \subset [0, 1]^d$. Let $(-\Delta)^s$ the Dirichlet fractional Laplacian (see Equation (1.2)) and $(\widetilde{-\Delta})^s$ the periodic fractional Laplacian (applied on the function restricted to $[0, 1]^d$). Then, for $x \in \Omega$, $S \in (1, \infty)$, we have*

$$S^{-2s} \left((\widetilde{-\Delta})^s u(S \cdot) \right) (x/S) = (-\Delta)^s u(x) + \mathcal{O} \left(S^{-(d+2s)} \right). \quad (3.1)$$

The periodic fractional Laplacian can be discretized using the DFT. A comprehensive overview is provided in [5]. Briefly repeated, the N^d -point discrete Fourier transformation of a vector $\mathbf{x} \in \mathbb{R}^{N^d}$ is defined as

$$(\text{DFT}_N \mathbf{x})_k = \hat{x}_k = \sum_{j_1=0}^{N-1} \cdots \sum_{j_d=0}^{N-1} x_j e^{-i \frac{2\pi j \cdot k}{N}} \quad (3.2)$$

and the inverse discrete Fourier transform is

$$(\text{IDFT}_N \hat{\mathbf{x}})_k = x_k = \frac{1}{N^d} \sum_{j_1=0}^{N-1} \cdots \sum_{j_d=0}^{N-1} \hat{x}_j e^{i \frac{2\pi j \cdot k}{N}}. \quad (3.3)$$

If the size N of the DFT is obvious, we will omit the subscript index N . The N^d -point discrete periodic fractional Laplacian of $u : [0; 1]^d \rightarrow \mathbb{R}$ is calculated via

$$\left((\widetilde{-\Delta})_N^s u \right) (x_\kappa) = (\text{IDFT}_N (\zeta \circ \text{DFT}_N f))(\kappa)$$

where \circ denotes the point-wise product, DFT and IDFT the N^d -point discrete Fourier transformation and

$$\zeta_k = |2\pi k|^{2s}.$$

Note that usual FFT implementations of the DFT calculate the discrete spectrum of f in the range $\{0, \dots, N-1\}^d$. To have the factors ζ at the correct scale, one has to shift the Fourier coefficients periodically to the interval $\{-N/2, \dots, N/2-1\}$ to obtain

$$\begin{aligned} \left((-\widetilde{\Delta})_{N^d}^s u \right) (x_\kappa) &= (\text{IDFT}_N(\zeta \circ \text{DFT}_N u))(\kappa) \\ &= \frac{1}{N^d} \sum_{k_1=-N/2}^{N/2-1} \cdots \sum_{k_d=-N/2}^{N/2-1} |2\pi k|^{2s} \hat{u}_k e^{i \frac{2\pi k \cdot \kappa}{N}}. \end{aligned}$$

We calculate the discretized scaled periodic fractional Laplacian in equation (3.1) similarly using the SN -point DFT and inverse DFT as follows: we extend the vector

$$\mathbf{u} = (u_k)_{k \in \mathcal{I}_N^d} \in \mathbb{R}^{N^d}, u_k = u(k/N)$$

to a vector

$$\bar{\mathbf{u}} = (\bar{u}_k)_{k \in \mathcal{I}_{SN}^d} \in \mathbb{R}^{(SN)^d}, \bar{u}_k = \begin{cases} u_k & \text{if } k < N \\ 0 & \text{otherwise} \end{cases}$$

where the $<$ -sign is meant component-wise and obtain

$$\left((-\widetilde{\Delta})_{S,N}^s u \right) (x_\kappa) = (\text{IDFT}_{SN}(\zeta \circ \text{DFT}_{SN} u))(\kappa) \quad (3.4)$$

$$= \frac{1}{(SN)^d} \sum_{j_1=-SN/2}^{SN/2-1} \cdots \sum_{j_d=-SN/2}^{SN/2-1} |2\pi j|^{2s} \hat{u}_j e^{i \frac{2\pi j \cdot \kappa}{SN}} \quad (3.5)$$

$$= \frac{(2\pi)^{2s}}{(SN)^d} \sum_{j \in \mathcal{I}'_{SN}} |j|^{2s} \left(\sum_{k \in \mathcal{I}'_{SN}} u_k e^{-i \frac{2\pi j \cdot k}{SN}} \right) e^{i \frac{2\pi j \cdot \kappa}{SN}} \quad (3.6)$$

$$= \frac{(2\pi)^{2s}}{(SN)^d} \sum_{k \in \mathcal{I}'_N} u_k \sum_{j \in \mathcal{I}'_{SN}} |j|^{2s} e^{i \frac{2\pi}{SN} j \cdot (\kappa - k)}. \quad (3.7)$$

The last line is certainly not the most efficient way to evaluate $\left((-\widetilde{\Delta})_{S,N}^s u \right) (x_\kappa)$ – this should instead be done via the FFT algorithm as stated in the first line. However, the expression will be needed in the following to show an equivalence of the sinc-fractional Laplacian and the scaled periodic fractional Laplacian.

3.2. Equivalence of the scaled periodic fractional Laplacian and the sinc-fractional Laplacian. There is a certain equivalence of the discrete scaled periodic fractional Laplacian and the sinc-fractional Laplacian. Precisely, if the integration in the calculation of Φ , see equation (2.13) is done exactly, the N^d -point sinc-fractional Laplacian is the same as the N^d -point discrete scaled periodic fractional Laplacian with infinite scale factor. This is stated in the following Theorem 3.1.

Theorem 3.1. *Let $u \in C_c^\infty([0; 1]^d)$. Then, for $S \rightarrow \infty$*

$$S^{-2s} \left((-\widetilde{\Delta})_{S,N}^s u \right) (x_\kappa) \rightarrow \left((-\Delta)_N^s u \right) (x_\kappa)$$

Proof. Refer to equations (3.7), (2.9) to see that it is enough to show that

$$S^{-2s} \frac{(2\pi)^{2s}}{(SN)^d} \sum_{j \in \mathcal{I}'_{SN}} |j|^{2s} e^{i \frac{2\pi}{SN} j \cdot (\kappa - k)} \rightarrow \Phi^N(\kappa - k) \quad (3.8)$$

$\forall K := \kappa - k$ as $S \rightarrow \infty$. Indeed, we have

$$\Phi^N(\kappa - k) = (2\pi N)^{-d} \int_{D_N} |\omega|^{2s} e^{i\frac{\omega \cdot (\kappa - k)}{N}} d\omega$$

(see equation (2.13)) and for the left-hand side of (3.8), we have

$$\begin{aligned} & \frac{(2\pi)^{2s}}{N^d} S^{-(d+2s)} \sum_{j \in \mathcal{I}'_{S_N}} |j|^{2s} e^{i\frac{2\pi}{S} j \cdot K} \\ &= \frac{(2\pi)^{2s}}{N^d} S^{-(d+2s)} \sum_{j \in \mathcal{I}'_N} \sum_{i \in \mathcal{I}_S} |Sj + i|^{2s} e^{i\frac{2\pi}{S} (Sj+i) \cdot K} \\ &= \frac{(2\pi)^{2s}}{N^d} \sum_{j \in \mathcal{I}'_N} \sum_{i \in \mathcal{I}_S} S^{-d} |j + i/S|^{2s} e^{i\frac{2\pi}{N} (j+i/S) \cdot K} \\ &\xrightarrow{S \rightarrow \infty} \frac{(2\pi)^{2s}}{N^d} \sum_{j \in \mathcal{I}'_N} \int_{j_1}^{j_1+1} \cdots \int_{j_d}^{j_d+1} |\omega|^{2s} e^{i\frac{2\pi}{N} \omega \cdot K} \\ &= \frac{(2\pi)^{2s}}{N^d} \int_{[-\frac{N}{2}, \frac{N}{2}]^d} |\omega|^{2s} e^{i\frac{2\pi}{N} \omega \cdot K} d\omega \\ &= (2\pi N)^{-d} \int_{D_N} |\omega|^{2s} e^{i\frac{\omega \cdot K}{N}} d\omega \end{aligned}$$

which completes the proof. \square

A similar result is presented in [24] for functions with non-compact support using the semi-discrete Fourier transformation. In Section 3.3, see Theorem 3.2, we show a direct relation between simple quadrature rules to evaluate the discrete convolution kernel $\hat{\Phi}$ and scaled Fourier fractional Laplacians.

3.3. Setting up the convolution kernel. As stated before, we aim to calculate the discrete Fourier transformation $\hat{\Phi}$ of Φ directly, instead of having to calculate it as the DFT of Φ as the latter is hard to obtain. While the fast implementation of the convolution is standard and can be found in many textbooks, our contribution is the formulation that makes the use of fast convolution algorithms applicable. Therefore, let $\mathcal{I}'_{2N} = \{-N, \dots, (N-1)\}^d$ and $k \in \mathcal{I}'_{2N}$ a multiindex. Let $\Phi_k = (-\Delta)^s \varphi_N(x_k)$, $x_k = k/N \in \mathbb{R}^n$. Let $\hat{\Phi} = \text{DFT}_{2N}(\Phi)$ the discrete Fourier transform of $\Phi \in \mathbb{R}^{(2N)^d}$. We start the computation with the fact that

$$\hat{\Phi}_k = \sum_{j \in \mathcal{I}'_{2N}} \Phi_j e^{-i2\pi k \cdot j / (2N)} \quad (3.9)$$

$$= N^{2s} (2\pi)^{-d} \sum_{j \in \mathcal{I}'_{2N}^d} \left(\int_D |\omega|^{2s} e^{i\omega \cdot j} d\omega \right) e^{-i\pi k \cdot j / N} \quad (3.10)$$

$$= N^{2s} (2\pi)^{-d} \int_D |\omega|^{2s} \sum_{j \in \mathcal{I}'_{2N}} e^{ij \cdot (\omega - \frac{\pi}{N} k)} d\omega. \quad (3.11)$$

Where we use the definition of the discrete Fourier transformation in the first equation, see equation (3.2) and the formula for Φ_j , see equation (2.13), in the second equation.

For $x \in \mathbb{R}$, define

$$Y(x) := \sum_{j=-N}^{N-1} e^{ijx} \quad (3.12)$$

and observe that

$$Y(x) = \begin{cases} \frac{e^{-iNx}(e^{2iNx}-1)}{e^{ix}-1} & \text{if } e^{ix} - 1 \neq 0 \\ 2N & \text{otherwise.} \end{cases} \quad (3.13)$$

To simplify the sum in equation (3.11), we observe that for $x \in \mathbb{R}^d$, we have

$$\begin{aligned} \sum_{j \in \mathcal{I}'_{2N}} e^{ij \cdot x} &= \sum_{j_1=-N}^{N-1} \dots \sum_{j_d=-N}^{N-1} e^{i(j_1 x_1 + \dots + j_d x_d)} \\ &= \sum_{j_1=-N}^{N-1} e^{ij_1 x_1} \dots \sum_{j_d=-N}^{N-1} e^{ij_d x_d} \\ &= \prod_{i=1}^d Y(x_i), \end{aligned}$$

so define

$$Y_d(x) := \prod_{n=1}^d Y(x_n), \quad (3.14)$$

plug this into equation (3.11) and obtain

$$\hat{\Phi}_k = N^{2s}(2\pi)^{-d} \int_D |\omega|^{2s} \sum_{j \in \mathcal{I}'_{2N}} e^{ij \cdot (\omega - \pi/Nk)} d\omega \quad (3.15)$$

$$= N^{2s}(2\pi)^{-d} \int_D |\omega|^{2s} Y_d(\omega - \pi/Nk) d\omega \quad (3.16)$$

$$= \underbrace{N^{2s}(2\pi)^{-d} \left(\frac{\pi}{N}\right)^{d+2s}}_{=\pi^{2s} \cdot (2N)^{-d}} \int_{[-N;N]^d} |\omega|^{2s} Y_d\left(\frac{\pi}{N}(\omega - k)\right) d\omega. \quad (3.17)$$

Now, we have the same domains for k and ω . Finally, we note that the second factor $Y_d(\dots)$ in the integrand is periodic with the length $2N$ of the integrals and, thus, (3.11) can be implemented as

a convolution using the FFT algorithm and using quadrature rules as follows:

$$\hat{\Phi}_k = \underbrace{\pi^{2s}(2N)^{-d}}_{C(N,d,s)} \int_{[-N;N]^d} |\omega|^{2s} Y_d \left(\frac{\pi}{N} (\omega - k) \right) d\omega \quad (3.18)$$

$$= C(N, d, s) \sum_{j \in \mathcal{I}'_{2N}} \int_{[0;1]^d} |j + \omega|^{2s} Y_d \left(\frac{\pi}{N} (j + \omega - k) \right) d\omega \quad (3.19)$$

$$\approx C(N, d, s) \sum_{j \in \mathcal{I}'_{2N}} \sum_{i=1}^{N_Q} \alpha_i |j + x_i|^{2s} Y_d \left(\frac{\pi}{N} (j + x_i - k) \right) \quad (3.20)$$

$$= C(N, d, s) \sum_{i=1}^{N_Q} \alpha_i \sum_{j \in \mathcal{I}'_{2N}} |j + x_i|^{2s} Y_d \left(-\frac{\pi}{N} (k - j) + \frac{\pi}{N} x_i \right). \quad (3.21)$$

Where $(x_i, \alpha_i)_{i=1, \dots, N_Q}$ is a quadrature rule on $[0; 1]^d$. The inner sum can be obtained as a discrete convolution for each i using two forward and one backward DFTs. In summary, we have to execute $3N_Q$ DFTs of size $(2N)^d$ to obtain $\hat{\Phi}$. This is the computationally most demanding step in our algorithm, but it has to be performed only once when $\hat{\Phi}$ is applied multiple times. The values of $\hat{\Phi}$ could even be stored for given of N and s . It is also possible to reduce the sizes of the DFTs to $(2N - 1)^d$. This, however, complicates the preceding computations.

A consequence of Theorem 3.1 is that the exactness of the integration in Equation (3.21) is decisive for the accuracy of our method. A trivial choice for the integration points x_i and weights α_i is

$$x_i = \frac{i}{N_Q}, i \in \{0, \dots, N_Q - 1\}^d \text{ and } \alpha_i = \alpha = \frac{1}{N_Q^d}. \quad (3.22)$$

For this quadrature rule, the sinc-fractional Laplacian is exactly the same as the discrete scaled periodic fractional Laplacian with $S = 2N_Q$. We will discuss more possibilities along with numerical experiments in section 4.1.

Theorem 3.2. *If $\hat{\Phi}$ in equation (3.21) is calculated using the quadrature rule from equation (3.22), then with $S = 2N_Q$ we have for all κ that*

$$((-\Delta)_N^s u)(x_\kappa) = ((-\widetilde{\Delta})_{S,N}^s u)(x_\kappa)$$

Proof. We already derived that

$$((-\widetilde{\Delta})_{S,N}^s u)(x_\kappa) = \frac{(2\pi)^{2s}}{S^{2s} N S^d} \sum_{k \in \mathcal{I}'_N} u_k \underbrace{\sum_{j \in \mathcal{I}'_{NS}} |j|^{2s} e^{i \frac{2\pi j(\kappa - k)}{SN}}}_{= \tilde{\Phi}(\kappa - k)},$$

see 3.7. Using 2.9 one can verify that it is enough to show that

$$\Phi^N(\kappa - k) = \frac{(2\pi)^{2s}}{S^{2s} N S^d} \tilde{\Phi}(\kappa - k)$$

for an appropriate choice of $(\alpha_i, x_i)_{i=1, \dots, N_Q}$. From 3.21, we derive using 3.22 that

$$\hat{\Phi}_k = C(N, d, s) \frac{1}{N_Q^d} \sum_{j \in \mathcal{I}'_{2NN_Q}} \left| \frac{j}{N_Q} \right|^{2s} Y_d \left(\frac{\pi}{N} \left(\frac{j}{N_Q} - k \right) \right).$$

We then calculate the DFT of $\tilde{\Phi}$ and obtain

$$\begin{aligned}
 \hat{\Phi}_k &= \frac{(2\pi)^{2s}}{S^{2s}NS} \sum_{\kappa \in \mathcal{I}'_N^d} \tilde{\Phi}_\kappa e^{-i\frac{2\pi\kappa k}{2N}} \\
 &= \frac{(2\pi)^{2s}}{S^{2s}NS^d} \sum_{\kappa \in \mathcal{I}'_N^d} \left(\sum_{j \in \mathcal{I}'_{NS}^d} |j|^{2s} e^{i\frac{2\pi j\kappa}{SN}} \right) e^{-i\frac{2\pi\kappa k}{2N}} \\
 &= \frac{(2\pi)^{2s}}{S^{2s}NS^d} \sum_{j \in \mathcal{I}'_{NS}^d} |j|^{2s} Y \left(2\pi \left(\frac{j}{SN} - \frac{k}{2N} \right) \right) \\
 &= \frac{\pi^{2s}}{(2N)^d N_Q^d} \sum_{j \in \mathcal{I}'_{2NN_Q}^d} \left| \frac{j}{N_Q} \right|^{2s} Y \left(\frac{\pi}{N} \left(\frac{j}{N_Q} - k \right) \right),
 \end{aligned}$$

which completes the proof. \square

3.4. Solving the Dirichlet problem. In section 2.1, we have seen how to implement the application of the discrete operator Φ^N to a vector $\mathbf{u} \in \mathbb{R}^{N^d}$ efficiently using the fast Fourier transformation algorithm. In this section, we will show how this is used to solve the *fractional Poisson problem* with Dirichlet exterior conditions, i.e., (1.1), repeated here for convenience:

$$\text{find } u \text{ s.t. } \begin{cases} (-\Delta)^s u = f & \text{in } \Omega \\ u = 0 & \text{in } \mathbb{R}^d \setminus \Omega \end{cases} \quad (3.23)$$

where $\Omega \subset [0; 1)^d \subset \mathbb{R}^d$ is an arbitrary Lipschitz domain and f is a given function. Originally, our methods operates on the full cube $[0; 1)^d$. This leads to the discretized problem

$$\text{find } \mathbf{u} \in \mathbb{R}^{N^d} \text{ s.t. } \Phi^N \mathbf{u} = \mathbf{f} \quad (3.24)$$

where $\mathbf{f} = (f_k)_{k \in \mathcal{I}_N^d}$, $f_k = f(x_k)$, $x_k = k/N$ and Φ^N is the discrete operator from equation (2.9). As shown, the application of Φ^N to a vector $\mathbf{u} \in \mathbb{R}^{N^d}$ can be implemented efficiently using the fast Fourier transformation algorithm. It is thus feasible to solve (3.24) using iterative methods that work through subsequent applications of the operator instead of inverting them directly. In the present case, we use the conjugate gradient method [23] as it is fast, easy to implement and numerically stable. The same procedure has been used by Duo and Zhang in [20] to solve the fractional Poisson problem in two-and three dimensions on rectangular (or cuboid) domains using their finite difference method, and by Minden and Ying [28] to solve the discrete system they obtain using singularity subtraction. To overcome the issue of being restricted to the cube $\Omega = [0; 1)^d$ and solve problems on arbitrary domains $\Omega \subset [0; 1)^d$, we embed the domain into the cube and set the coefficients outside of Ω to 0. To implement this, we introduce a linear mapping

$$S_\Omega : \mathbb{R}^{N^d} \longrightarrow \mathbb{R}^{N^d}$$

such that for all $\mathbf{u} = (u_k)_{k \in \mathcal{I}_N^d} \in \mathbb{R}^{N^d}$

$$(S_\Omega \mathbf{u})_k = \begin{cases} u_k & \text{if } k/N \in \Omega \\ 0 & \text{otherwise} \end{cases}$$

holds. Additionally, we define $S_D := \mathbf{1} - S_\Omega$ where $\mathbf{1}$ is the identity on \mathbb{R}^{N^d} . Now, as we only want to solve (3.24) for the indices that belong to Ω , we solve the modified problem

$$\text{find } \mathbf{u} \in \mathbb{R}^{N^d} \text{ s.t. } \begin{cases} S_\Omega \Phi^N S_\Omega^T \mathbf{u} = S_\Omega \mathbf{f} \\ S_D u = 0 \end{cases} \quad (3.25)$$

instead. Note that this is not a system on \mathbb{R}^{N^d} anymore, but only on the subspace spanned by the indices that are selected by S_Ω . The calculations are still done on the full \mathbb{R}^{N^d} as this is the space where we can apply Φ^N efficiently, which is the prerequisite for using the conjugate gradient method. To show the capabilities of the methods, we apply it benchmark problems and problems arising from applications.

3.5. Summary of algorithms and computational complexity. In this section, we provide more details on the implementation of the algorithms. The indices in the following computations will be chosen such that they fit the indices of usual FFT implementations. All our implementations rely on the FFTW library [21]. Computing the discrete solution of the Dirichlet-exterior value problem (1.1) essentially consists of two steps.

- setup the discrete operator Φ^N
- solve the (discrete) system $S_\Omega \Phi^N S_\Omega^T \mathbf{u} = S_\Omega \mathbf{f}$.

Regarding the first step, we do not actually calculate Φ^N , but its DFT $\hat{\Phi}^N$ following the procedure described in section 3.3. Further details are provided in Algorithm 1. The arithmetic operations

Algorithm 1 Calculation of the convolution kernel

```

1: function CALC_PHI_HAT( $N, s, d$ )
2:    $\hat{\Phi} \leftarrow$  complex array of size  $(2N)^d$ , filled with 0
3:   for  $(x_i, \alpha_i) \in Q$  do
4:      $c_1 \leftarrow$  empty real array of size  $(2N)^d$ 
5:      $c_2 \leftarrow$  empty real array of size  $()^d$ 
6:     for  $j \in \mathcal{I}_{2N}$  do
7:        $c_1[j] \leftarrow |j - N\vec{1} + x_i|^{2s}$ 
8:        $c_2[j] \leftarrow Y_d(-\pi/N * (j - N\vec{1} + x_i))$ 
9:     end for
10:     $C_1 \leftarrow$  FFT( $c_1$ )
11:     $C_2 \leftarrow$  FFT( $c_2$ )
12:     $C \leftarrow C_1 * C_2$ 
13:     $c \leftarrow$  IFFT( $C$ )
14:    for  $k \in \mathcal{I}_{2N}$  do
15:       $E_k \leftarrow (2\pi)^{-d} * (\pi/N)^{d+2*s} * N^{2s} * \text{EXP}(i\pi(k_1 + \dots + k_d))$ 
16:       $\hat{\Phi}[k] \leftarrow \hat{\Phi}[k] + \alpha_i * E_k * c[k]$ 
17:    end for
18:  end for
19:  return  $\hat{\Phi}$ 
20: end function

```

$*$, $+$ are meant component-wise if applied to arrays. The computationally most demanding part in Algorithm 1 is the 3-fold execution of the FFT-algorithm in lines 10, 11 and 13, which are needed

to compute the inner sum on the right-hand side of equation (3.21), i.e., the convolution. These FFTs have to be executed for each of the quadrature points, i.e., N_Q -times and they are of size $(2N)^d$. However, this is done for all the $k \in \mathcal{I}_{2N}^d$ at a total cost of $\mathcal{O}((2N)^d \log((2N)^d))$ which is still small compared to a naive implementation at cost $\mathcal{O}(((2N)^d)^2)$.

For the second step, i.e., the solution of the fractional PDE, we use the conjugate gradient (CG) method. The method solves a linear system

$$\mathbf{A}\mathbf{u} = \mathbf{b}, \quad \mathbf{b} \in \mathbb{R}^N, \mathbf{A} \in \mathbb{R}^{N \times N} \text{ invertible}$$

via successive applications of the matrix \mathbf{A} instead of solving it directly.

Consequently, the algorithm is fast if the application of the operator \mathbf{A} can be calculated efficiently. This is the case in our setting, since we need to compute the application (convolution) of Φ^N to a vector \mathbf{u} . As mentioned above, we do so by using FFT based algorithms in order to reduce the computational complexity. We have to introduce some padding in order to apply the zero-padding convolution instead of circular convolution as the FFT based algorithm would normally do. The details are provided in Algorithm 2.

Algorithm 2 Application of Φ^N

```

1: function APPLY_PHI( $\mathbf{u}$ ,  $\hat{\Phi}^N$ )
2:    $\bar{\mathbf{u}} \leftarrow$  complex array of size  $(2N)^d$ , filled with 0
3:   for  $k \in \mathcal{I}_N$  do
4:      $\bar{\mathbf{u}}[k + N\bar{\mathbf{1}}] \leftarrow \mathbf{u}[k]$ 
5:   end for
6:    $\hat{\mathbf{u}} \leftarrow \text{FFT}(\bar{\mathbf{u}})$ 
7:   for  $k \in \mathcal{I}_{2N}$  do
8:      $\hat{\mathbf{u}}[k] \leftarrow \hat{\mathbf{u}}[k] * \hat{\Phi}[k]$ 
9:   end for
10:   $\hat{\mathbf{f}} \leftarrow \text{IFFT}(\hat{\mathbf{u}})$ 
11:   $\mathbf{f} \leftarrow$  empty real array of size  $N^d$ 
12:  for  $k \in \mathcal{I}_N$  do
13:     $\mathbf{f}[k] \leftarrow \hat{\mathbf{f}}[k]$ 
14:  end for
15:  return  $\mathbf{f}$ 
16: end function

```

If the domain in the exterior value problem is the full cube $[0; 1]^d$, we can simply use the conjugate gradient method with the operator Φ^N using the efficient application described in Algorithm 2. If we want to restrict the exterior value problem to a domain $\Omega \subsetneq [0; 1]^d$, we use the strategy described in section 3.4 and further summarized in Algorithm 3. Both the operator Φ^N and the operator restricted to a smaller area can be applied to a vector \mathbf{u} at cost $\mathcal{O}((2N)^d \log((2N)^d))$ which is substantially less than the cost $\mathcal{O}(((2N)^d)^2)$ of the naive implementation.

4. NUMERICAL EXPERIMENTS

We present four numerical examples to demonstrate the efficiency of our implementation. First, we compare the scaled periodic fractional Laplacian (see section 3.1) to the sinc-fractional Laplacian

Algorithm 3 Application of Φ with restriction to $\Omega \subset [0; 1]^d$

```

1: function APPLY_PHI_OMEGA( $\mathbf{u}, \hat{\Phi}^N$ )
2:    $\mathbf{S} \leftarrow$  empty real array of size  $N^d$ 
3:   for  $k \in \mathcal{I}_N$  do
4:     if  $k/N \in \Omega$  then
5:        $\mathbf{S}[k] \leftarrow 1$ 
6:     else
7:        $\mathbf{S}[k] \leftarrow 0$ 
8:     end if
9:   end for
10:  for  $k \in \mathcal{I}_N$  do
11:     $\mathbf{u}[k] \leftarrow \mathbf{u}[k] * \mathbf{S}[k]$ 
12:  end for
13:   $\mathbf{f} \leftarrow$  APPLY_PHI( $\mathbf{u}, \hat{\Phi}^N$ )
14:  for  $k \in \mathcal{I}_N$  do
15:     $\mathbf{f}[k] \leftarrow \mathbf{f}[k] * \mathbf{S}[k]$ 
16:  end for
17:  return  $\mathbf{f}$ 
18: end function

```

for different scaling factors. Section 4.2 provides an experimental error analysis for a case where analytic solutions of the Dirichlet problem are known explicitly. As an example for the importance of using the correct exterior value conditions, we compare the fractional Allen-Cahn evolution equation for the periodically extended and the Dirichlet case in section 4.3. Finally, in section 4.4, we show an application to image denoising as introduced in [5].

4.1. Quadrature rules for the convolution kernel. In this section, we want to numerically evaluate how different quadrature rules in the calculation of the convolution kernel behave. For that reason, we calculate the discrete scaled periodic Fractional Laplacian $(-\Delta)_{S,N}^s$ of a function u with different scaling factors S and compare it to the sinc-fractional Laplacian $(-\Delta)_N^s$ of u computed using different quadrature rules in the integration in equation (3.21).

We obtain the simple error estimate

$$\|(-\Delta)^s u - (-\Delta)_N^s u\| \leq \|(-\Delta)^s u - (\widetilde{-\Delta})_{S,N}^s u\| + \|(\widetilde{-\Delta})_{S,N}^s u - (-\Delta)_N^s u\| \quad (4.1)$$

From Lemma 3.1, we know that the first term is $\mathcal{O}(S^{-d+2s})$, and the second term can be calculated using the methods presented in sections 2.2, 3.1, and 4.1.

In order to obtain good accuracy for calculating the sinc-fractional Laplacian at a reasonable computational cost, we aim to use better quadrature rules than the naive one presented in equation (3.22).

Basically, we can use any quadrature rule, but for efficient implementation, we should use the same quadrature rule on each of the d -dimensional cubes $[j_1; j_1 + 1] \times \cdots \times [j_d; j_d + 1]$. This causes some issues as some cubes contain an integrand with a singularity due to the factor $|j + \omega|^{2s}$ if $j_i \in \{-1, 0\}$ for some $i \in \{1, \dots, d\}$. Nevertheless, we obtain good results using a Gauß-Legendre quadrature rule. On cubes, we thus employ an n^d -point tensor product Gauß-Legendre quadrature. The results are illustrated in Figure 1, where we show the second term in the estimate (4.1). Due to Theorem 3.1, a sinc-fractional Laplacian with exactly computed convolution kernel corresponds

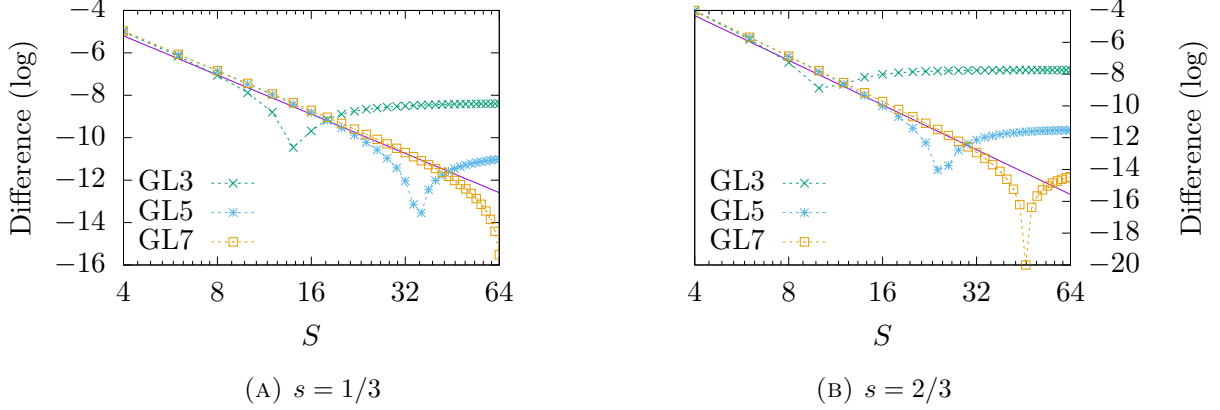


FIGURE 1. Comparison of the scaled periodic fractional Laplacian and our implementation of the sinc-fractional Laplacian applied to a standard mollifier with support in $[0; 1)^d$ for fixed $N = 128$. The solid purple line shows the rate $\mathcal{O}(S^{-d+2s})$. GL3, GL5 and GL7 denote Gauss-Legendre integration with 3, 5 and 7 points in each spatial direction.

to a periodic fractional Laplacian with ‘infinite’ scaling. In that case the difference between the sinc-fractional Laplacian and the $(-\Delta)_{S,N}^s$ would decrease at the rate $\mathcal{O}(S^{-d+2s})$. In the figure, one can see that this rate applies until the quadrature errors from the computation of the convolution kernel dominate. Naturally, this happens later for more exact quadratures.

4.2. Function with constant fractional Laplacian on the unit sphere. One of the few examples where the solution to the fractional Laplace Dirichlet problem is known explicitly is the problem

$$\text{find } u \text{ s.t. } \begin{cases} (-\Delta)^s u = 1 & \text{in } \Omega \\ u = 0 & \text{in } \mathbb{R}^d \setminus \Omega. \end{cases} \quad (4.2)$$

For $\Omega = \{x \in \mathbb{R}^d \mid |x| < 1\}$, the solution to (4.2) is given by (see [13])

$$u = C_u(d, s) \max 0, (1 - |x|)^s \quad (4.3)$$

where

$$C_u(d, s) = \left(\frac{2^{2s} \cdot \Gamma(\frac{d}{2} + s) \Gamma(1 + s)}{\Gamma(\frac{d}{2})} \right)^{-1}. \quad (4.4)$$

After shifting and scaling the problem to a disc or a sphere that is a subset of the cube $[0; 1)^d$, and using the method from section 3.4, we obtain the results shown in Figure 4 in the case $d = 2$, which clearly resemble the expected results. In Figure 3, we show the number of iterations the conjugate gradient method required until the residual

$$\|\mathbf{r}\|_{L^2} = \frac{1}{N^d} \sum_{k \in \mathcal{I}_N^d} r_k^2$$

dropped below 10^{-8} . Since the conditioning of the problem becomes worse for finer grid resolution, it is expected that more iterations are necessary for increasing N . The scaling of the number of iterations can be seen in Table 2. We note that for lower fractional exponent s , the required number

of iterations is lower – this is reasonable as the largest eigenvalue of the sinc-fractional Laplacian should scale like N^{2s} .

TABLE 2. Scaling of the number of CG-iterations depending on grid size. We fit the graph in Figure 3 to the law N^β .

s	1/4	1/3	1/2	2/3	3/4
β	0.2600	0.3391	0.4879	0.6501	0.7298

Figure 5 shows the results when $d = 3$.

As a numerical analysis of our method is still pending and remains part of future work, we experimentally evaluate the capabilities of our method. For that, we solve problem (4.2) for different values of s on grids of increasing size N^d for $d = 2$ and $d = 3$. We approximate the L_2 -error as

$$\|u_N - u\|_2 \approx \sqrt{\frac{1}{N^d} \sum_k (u_k - u(x_k))^2},$$

where $u_N = \sum_{k \in \mathcal{I}_N^d} u_k \varphi_k^N$ is the solution computed using the sinc-fractional Laplacian and u is the known analytic solution. The results can be seen in Figure 2 (top) for the $2d$ -case and in Figure 2 (bottom) for the $3d$ -case. In the $2d$ -case, we experimentally obtain the convergence rates shown in Table 3. The rates clearly correspond to the rates predicted in [2] by Acosta and Borthagaray, which are $\mathcal{O}(h^{\min(1, s+1/2)})$.

TABLE 3. Experimentally determined convergence rates.

s	1/4	1/3	1/2	2/3	3/4
Determined rate	0.7329	0.8192	0.9622	1.0166	1.0189
Expected rate	0.7500	0.8300	1.0000	1.0000	1.0000

4.3. Fractional Allen-Cahn equation. As a practical application that shows that our method correctly implements the Dirichlet exterior value conditions instead of periodic exterior value conditions, we calculate the evolution of the fractional Allen-Cahn equation

$$\partial_t u + (-\Delta)^{\frac{1}{2}} u = -\frac{1}{\varepsilon} W'(u)$$

for $\varepsilon = 2 \cdot 10^{-3}$; as an example here for fractional exponent $s = \frac{1}{2}$. The function $W: \mathbb{R} \rightarrow \mathbb{R}$ is a typical quartic double well potential of the form $W(u) = \frac{1}{4}u^2(u-1)^2$.

It has recently been proved [4, 31] that, for $\varepsilon \rightarrow 0$, the associated energy $\frac{1}{\log \varepsilon} \left([u]_{H^{\frac{1}{2}}}^2 + \frac{1}{\varepsilon} W(u) \right)$ converges (modulo constants) in the sense of Γ -convergence to the perimeter (in our one-dimensional case, a jump set counting functional). Heuristically, this energy prefers states of $u \in \{0, 1\}$. The fractional Sobolev norm ensures that transitions between these two states can not take place arbitrarily rapidly in space.

The gradient flow, accelerated by a factor of $\frac{1}{\varepsilon \log \varepsilon}$ as computed here, converges in one spatial dimension to a kink-antikink annihilation-type dynamic [22]. Again, heuristically, two nearby states close to $u = +1$, separated by a gap where $u = 0$, attract each other due to the long range

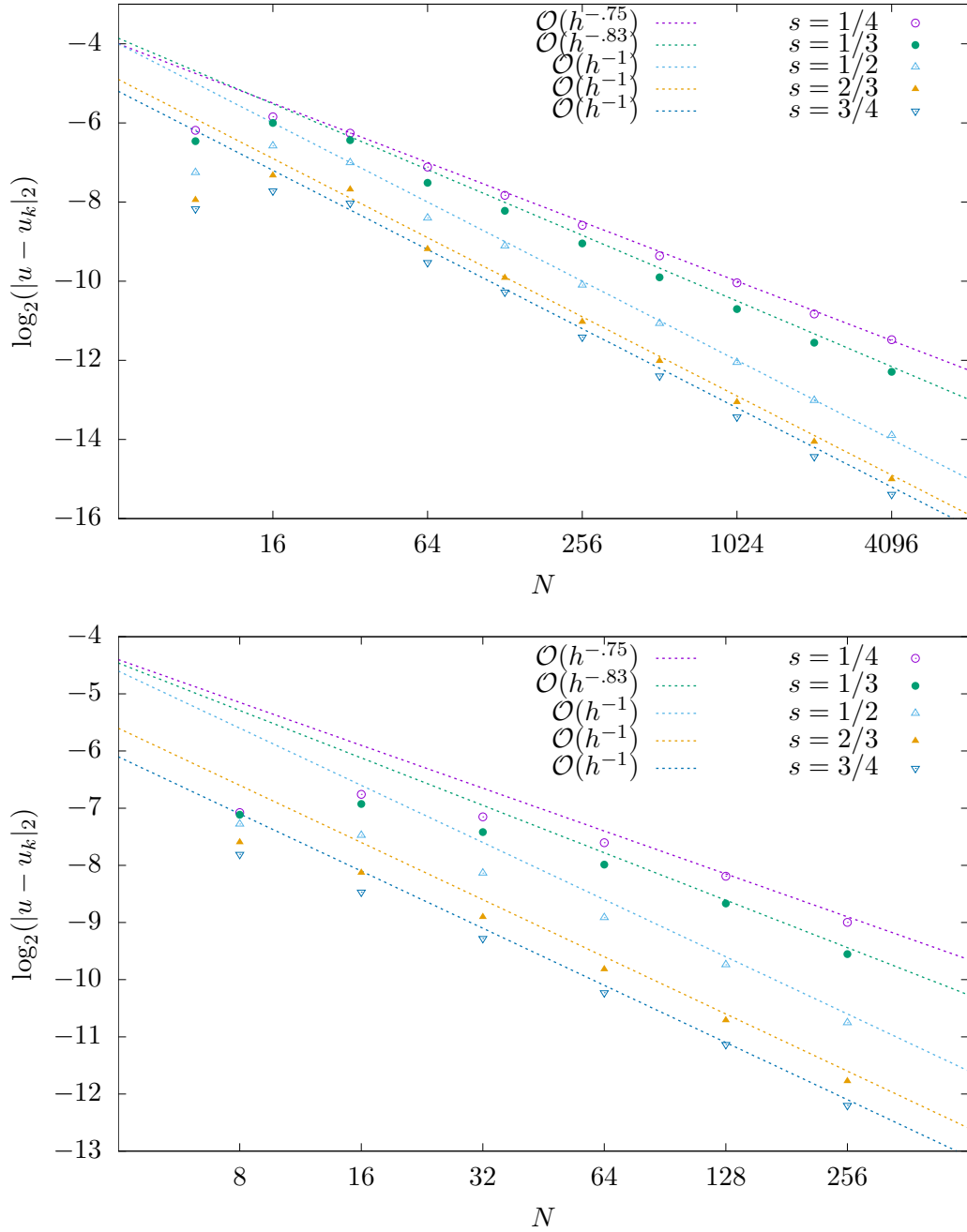


FIGURE 2. Experimental convergence analysis as a log-log plot in 2 dimensions (top) and 3 dimensions (bottom). The decay conforms to the rates predicted in [2] by Acosta and Borthagaray. N is the number of grid points in each direction, i.e., the total number of grid points is N^2 and N^3 in respectively.

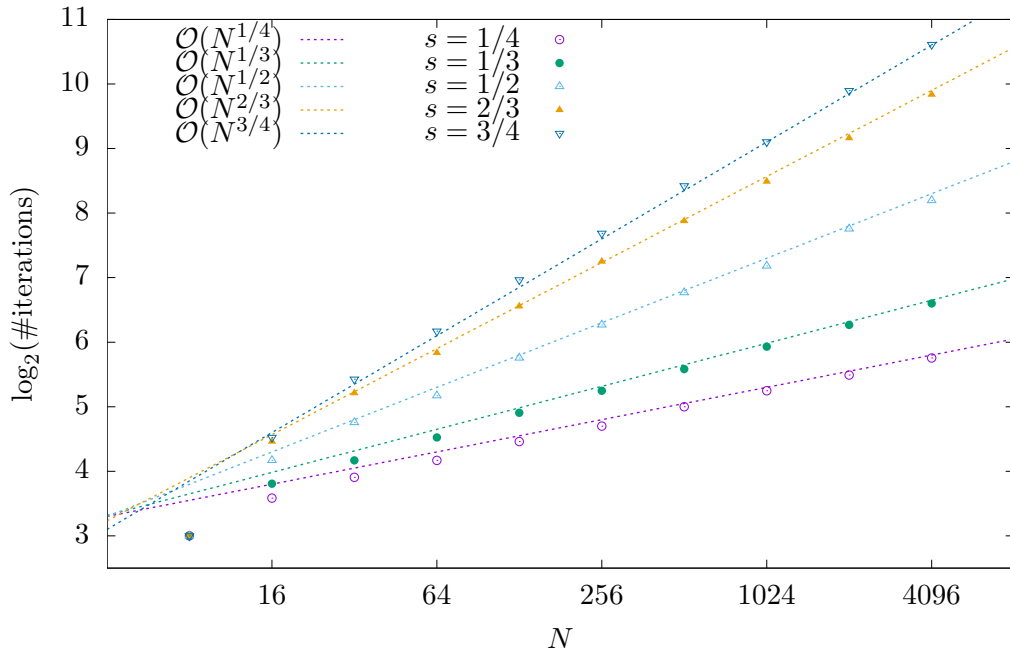


FIGURE 3. Number of iterations until convergence of the CG-method for the $2d$ -problem.

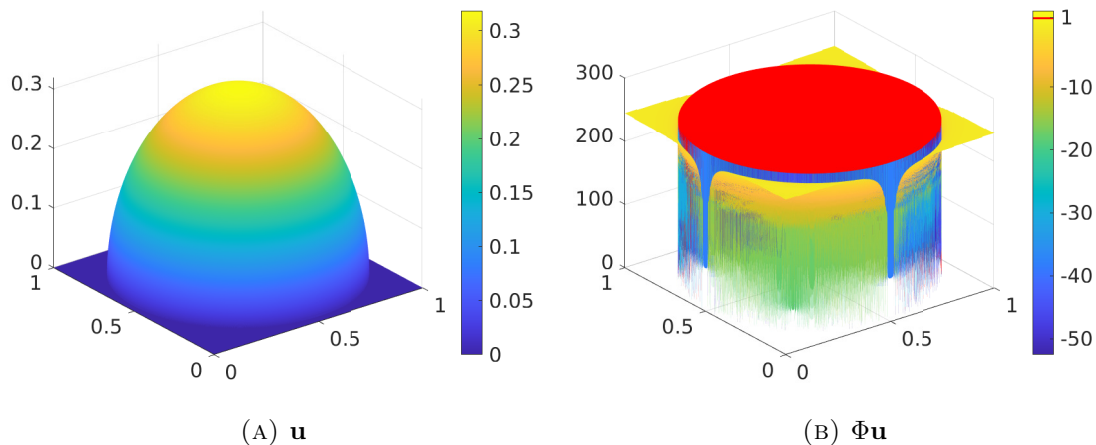


FIGURE 4. Discrete solution \mathbf{u} (A) and $\Phi\mathbf{u}$ (B) for problem 4.2 with $s = 1/2$ using $2^{12} \times 2^{12}$ grid points. The solution clearly resembles the expected solution, given in equation 4.3. In (B), values closer than $\varepsilon = 10^{-5}$ to 1 are colored red to show that the sinc-fractional Laplacian is constant in the correct region.

interaction via the fractional operator, so the two phase transitions (or kinks) move closer to each other. The expected behavior in the $\varepsilon \rightarrow 0$ limit is a kink velocity proportional to the reciprocal of the distance to the antikink (and vice-versa).

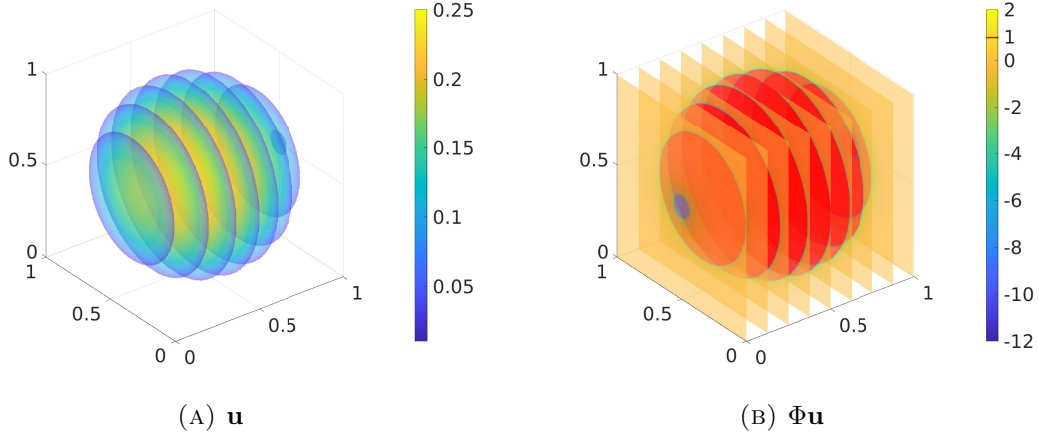


FIGURE 5. Discrete solution \mathbf{u} (A) and $\Phi\mathbf{u}$ (B) for problem 4.2 with $s = 1/2$ using $(2^8)^3$ grid points. In (B), values closer than $\varepsilon = 10^{-5}$ to 1 are colored red to show that the sinc-fractional Laplacian is constant in the correct region.

Note that the evolution for small $\varepsilon > 0$ is substantially faster than for the classical local Allen-Cahn equation, where exponentially slow kink-antikink annihilation was shown [12, 15].

We discretize the equation in time using an implicit Euler scheme with time step τ and obtain

$$\left(\mathbf{1} + \tau(-\Delta)^{\frac{1}{2}}\right) \mathbf{u}^{t+1} = -\frac{\tau}{\varepsilon} W'(\mathbf{u}^t) + \mathbf{u}^t. \quad (4.5)$$

To illustrate the differences due to exterior domain conditiong, we choose either the periodic fractional Laplacian or the sinc-fractional Laplacian and compare. In the first case, the system (4.5) can be solved directly using the discrete Fourier transformation, see, e.g., [5] for details. In the case of the sinc-fractional Laplacian, we use the conjugate gradient method as explained in section 3.4. We choose the domain $\Omega = [0; 1] \subset \mathbb{R}$ and

$$\mathbf{u}^0(x) = \chi_{[1/4; 3/4]}(x),$$

i.e., the indicator function on the interval $[\frac{1}{4}; \frac{3}{4}]$. In Figure 6, we show the evolution for different times. It can be clearly seen that the solution for periodic conditions reaches a steady state, due to symmetry: the attraction of the kink and antikink at $x = \frac{1}{4}$ and $x = \frac{3}{4}$, respectively is balanced by the attraction to their periodic mirror images past the domain boundary. In the case of the true Dirichlet problem, the annihilation is clearly visible. Figure 7 shows the time-evolution of the total mass (i.e., $m(t) = \int_0^1 u(x, t) dx$) as well as the position of the left kink (or phase transition) over time. The fit to the solution of the aforementioned limit equation (which is of the form $a\sqrt{t_0 - t}$ with parameters a and t_0) is included on the left panel in Figure 7.

4.4. Image denoising. In [5], Antil and Bartels have proposed to solve an image denoising variational problem. Given a noisy image g , it amounts to: $\min_u \frac{1}{2} \int_{\Omega} |(-\Delta)^{\frac{\alpha}{2}} u|^2 + \frac{\alpha}{2} \int_{\Omega} |u - g|^2$, i.e., they use the fractional Laplacian as the regularizer. Here $\alpha > 0$ is the regularization parameter. Starting from the seminal work of Rudin-Osher-Fatemi [30], where they used the total variation as a regularizer, such variational models are being regularly used in imaging science. The key advantage of the fractional Laplacian regularizer from [5] is the fact that one arrives at the following *linear*

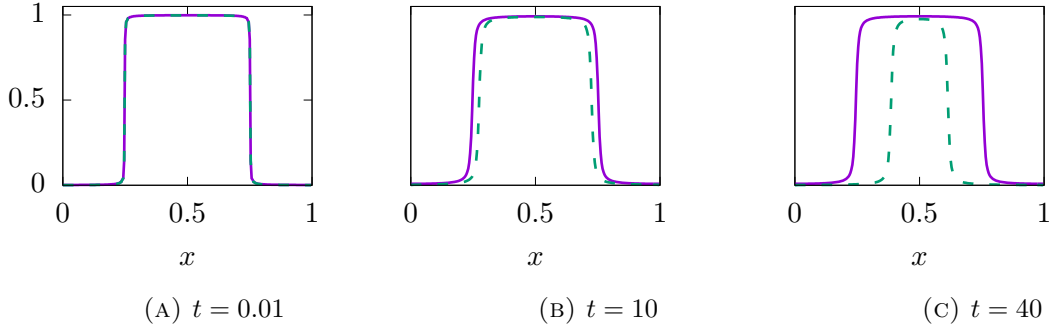


FIGURE 6. The solution $u(x, t)$ of the fractional Allen-Cahn equation for different times t . The solid purple line shows the evolution for the sinc-fractional Laplacian, dashed green line the evolution for the periodic fractional Laplacian.

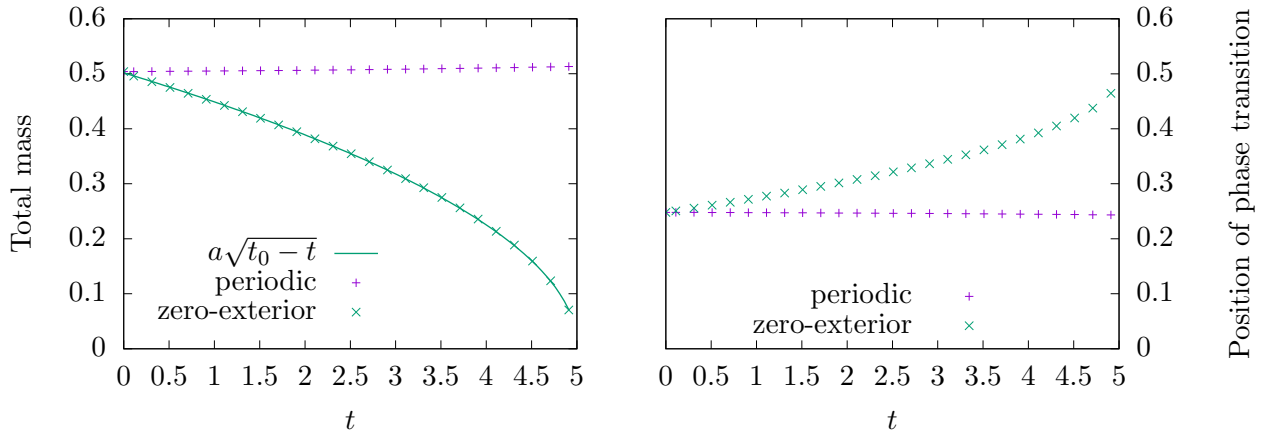


FIGURE 7. Evolution of the total mass (i.e., the integral of u) in the interval $[0; 1]$ (left) and of the position of the first phase transition (right) using both the periodic and the zero-exterior value Dirichlet (sinc)-fractional Laplacian for the fractional Allen-Cahn Equation. The continuous line in the left panel shows a fit to a square-root function $a\sqrt{t_0 - t}$, with $a = 0.2242$, $t_0 = 5.0104$

Euler-Lagrange equations:

$$(-\Delta)^s u + \alpha(g - u) = 0. \quad (4.6)$$

In the respective work, the authors use the spectral fractional Laplacian which applies periodic boundary conditions. In contrast, we use our method that uses Dirichlet-exterior value conditions. Here, we subtract the mean \bar{g} of g from g before the calculations and add it back afterwards. The results can be seen in Figures 8 and 9. The goal of this example is not to further illustrate the effectiveness of fractional Laplacian as a regularizer, but to show that we can obtain comparable results using the approach considered in this paper. This clearly follows from our example.

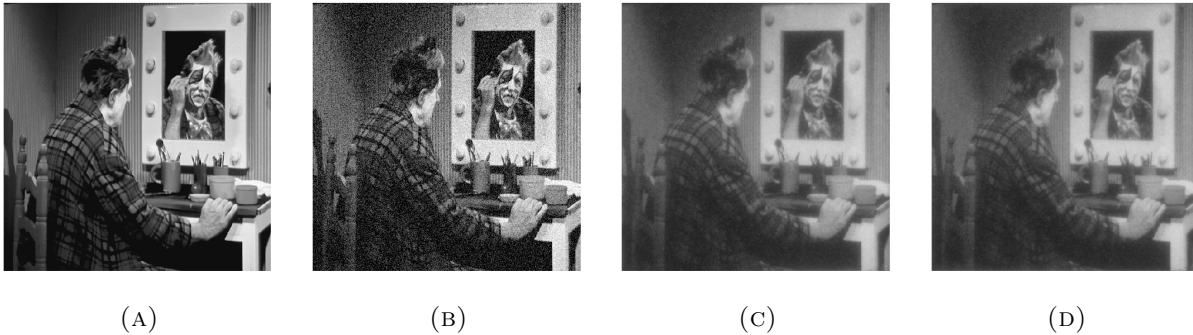


FIGURE 8. (A) Original image, (B) image corrupted with Gaussian noise, (C) denoised image using our method, and (D) the image denoised with the spectral method from [5]. We chose $s = 0.42$ and $\alpha = 10 \cdot 2\pi$.

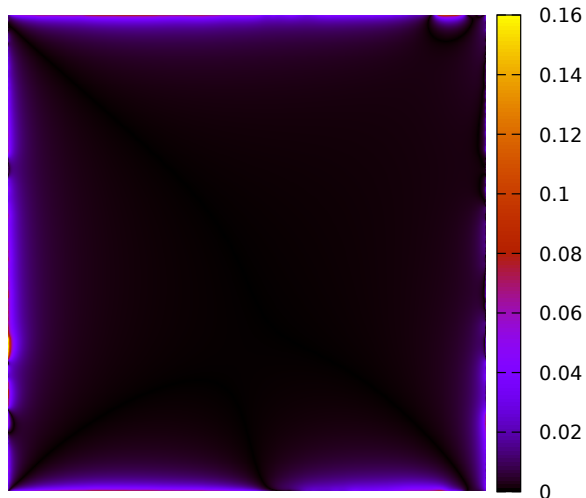


FIGURE 9. The difference of the image denoised with our method and denoised with the spectral method of [5] (see Figure 8). The differences clearly concentrate at the boundary of the images as one would expect.

5. CONCLUSION AND FUTURE WORK

The paper introduces a novel spectral method which efficiently allows application of the fractional Laplacian and a solution algorithm for fractional partial differential equations in $\mathcal{O}(N \log(N))$ operations. The proposed method works in both $2d$ and $3d$. We have further shown the effectiveness of method on two applications: a fractional Allen-Cahn and an image denoising problem. In both cases, we obtain expected results.

This work opens up new opportunities for problems where nonlocal operators such as fractional Laplacians appear, especially in $3d$. There are several open questions which we plan to tackle in future: (i) How to extend the proposed method to other exterior conditions such as Neumann or Robin and how to handle nonzero exterior conditions; (ii) A complete numerical analysis of the proposed method is currently missing; (iii) We have applied the proposed method to both linear

elliptic and nonlinear parabolic (Allen-Cahn) equations, it will also be interesting to carry out analysis in the nonlinear setting of Allen-Cahn; (iv) It will be interesting to apply the proposed method to equilibrium problems such as variational inequalities and PDE constrained optimization problems.

REFERENCES

- [1] N. Abatangelo and E. Valdinoci. Getting acquainted with the fractional Laplacian. In *Contemporary research in elliptic PDEs and related topics*, volume 33 of *Springer INdAM Ser.*, pages 1–105. Springer, Cham, 2019.
- [2] G. Acosta and J. P. Borthagaray. A fractional Laplace equation: regularity of solutions and finite element approximations. *SIAM Journal on Numerical Analysis*, 55(2):472–495, Jan 2017.
- [3] M. Ainsworth and C. Glusa. *Towards an efficient finite element method for the integral fractional Laplacian on polygonal domains*, pages 17–57. Springer International Publishing, Cham, 2018.
- [4] G. Alberti, G. Bouchitté, and P. Seppecher. Un résultat de perturbations singulières avec la norme $H^{1/2}$. *Comptes Rendus de l'Académie des Sciences. Série I. Mathématique*, 319(4):333–338, 1994.
- [5] H. Antil and S. Bartels. Spectral approximation of fractional PDEs in image processing and phase field modeling. *Computational Methods in Applied Mathematics*, 17, 04 2017.
- [6] H. Antil, Z. W. Di, and R. Khatri. Bilevel optimization, deep learning and fractional Laplacian regularization with applications in tomography. *Inverse Problems*, 36(6):064001, may 2020.
- [7] H. Antil, R. Khatri, and M. Warma. External optimal control of nonlocal PDEs. *Inverse Problems*, 35(8):084003, 35, 2019.
- [8] H. Antil and C. Rautenberg. Sobolev spaces with non-Muckenhoupt weights, fractional elliptic operators, and applications. *SIAM J. Math. Anal.*, 51(3):2479–2503, 2019.
- [9] G. Baumann and F. Stenger. Fractional calculus and sinc methods. *Fractional Calculus and Applied Analysis*, 14(4), jan 2011.
- [10] A. Bonito, J. P. Borthagaray, R. H. Nochetto, E. Otárola, and A. J. Salgado. Numerical methods for fractional diffusion. *Comput. Vis. Sci.*, 19(5-6):19–46, 2018.
- [11] A. Bonito, W. Lei, and J. E. Pasciak. Numerical approximation of the integral fractional Laplacian. *Numer. Math.*, 142(2):235–278, 2019.
- [12] L. Bronsard and R. V. Kohn. On the slowness of phase-boundary motion in one space dimension. *Communications on Pure and Applied Mathematics*, 43(8):983–997, Dec. 1990.
- [13] C. Bucur and E. Valdinoci. *Nonlocal diffusion and applications*. Springer, 2016.
- [14] L. Caffarelli and L. Silvestre. An extension problem related to the fractional Laplacian. *Communications in Partial Differential Equations*, 32, 08 2006.
- [15] J. Carr and R. L. Pego. Metastable patterns in solutions of $u_t = \varepsilon 2u_{xx} - f(u)$. *Communications on Pure and Applied Mathematics*, 42(5):523–576, 1989.
- [16] C. Cattani. Shannon wavelets theory. *Math. Probl. Eng.*, pages Art. ID 164808, 24, 2008.
- [17] C. Cattani. Local fractional calculus on Shannon wavelet basis. In *Fractional dynamics*, pages 6–30. De Gruyter Open, Berlin, 2015.
- [18] C. Cattani. Sinc-fractional operator on Shannon wavelet space. *Frontiers in Physics*, 6:118, 2018.
- [19] E. Di Nezza, G. Palatucci, and E. Valdinoci. Hitchhiker’s guide to the fractional sobolev spaces. *Bulletin des Sciences Mathématiques*, 136:521–573, 07 2012.
- [20] S. Duo and Y. Zhang. Accurate numerical methods for two and three dimensional integral fractional Laplacian with applications. *Computer Methods in Applied Mechanics and Engineering*, 355:639 – 662, 2019.
- [21] M. Frigo and S. G. Johnson. The design and implementation of FFTW3. *Proceedings of the IEEE*, 93(2):216–231, 2005. Special issue on “Program Generation, Optimization, and Platform Adaptation”.
- [22] M. d. M. González and R. Monneau. Slow motion of particle systems as a limit of a reaction-diffusion equation with half-Laplacian in dimension one. *Discrete and Continuous Dynamical Systems. Series A*, 32(4):1255–1286, 2012.
- [23] M. R. Hestenes and E. Stiefel. Methods of conjugate gradients for solving linear systems. *J Res NIST*, 49(6):409–436, 1952.
- [24] Y. Huang and A. Oberman. Finite difference methods for fractional Laplacians. *arXiv e-prints*, page arXiv:1611.00164, Nov. 2016.

- [25] A. Lischke, G. Pang, M. Gulian, F. Song, C. Glusa, X. Zheng, Z. Mao, W. Cai, M. M. Meerschaert, M. Ainsworth, and G. E. Karniadakis. What is the fractional laplacian? a comparative review with new results. *Journal of Computational Physics*, 404:109009, 2020.
- [26] J. McNamee, F. Stenger, and E. L. Whitney. Whittaker’s cardinal function in retrospect. *Math. Comp.*, 25:141–154, 1971.
- [27] D. Meidner, J. Pfefferer, K. Schürholz, and B. Vexler. *hp*-finite elements for fractional diffusion. *SIAM J. Numer. Anal.*, 56(4):2345–2374, 2018.
- [28] V. Minden and L. Ying. A simple solver for the fractional Laplacian in multiple dimensions. *SIAM Journal on Scientific Computing*, 42(2):A878–A900, 2020.
- [29] R. H. Nochetto, E. Otárola, and A. J. Salgado. A PDE approach to fractional diffusion in general domains: a priori error analysis. *Found. Comput. Math.*, 15(3):733–791, 2015.
- [30] L. I. Rudin, S. Osher, and E. Fatemi. Nonlinear total variation based noise removal algorithms. *Physica D: Nonlinear Phenomena*, 60(1):259 – 268, 1992.
- [31] O. Savin and E. Valdinoci. Γ -convergence for nonlocal phase transitions. *Annales de l’Institut Henri Poincaré. Analyse Non Linéaire*, 29(4):479–500, 2012.
- [32] F. Stenger. Summary of sinc numerical methods. *Journal of Computational and Applied Mathematics*, 121(1):379 – 420, 2000.
- [33] F. Stenger. *Handbook of Sinc Numerical Methods*. CRC Press, Inc., USA, 2010.
- [34] P. R. Stinga and J. L. Torrea. Extension problem and Harnack’s inequality for some fractional operators. *Communications in Partial Differential Equations*, 35(11):2092–2122, 2010.
- [35] E. Valdinoci. From the long jump random walk to the fractional Laplacian. *Bol. Soc. Esp. Mat. Apl. SeMA*, (49):33–44, 2009.
- [36] C. Weiss, B. van Bloemen Waanders, and H. Antil. Fractional operators applied to geophysical electromagnetics. *Geophysical Journal International*, 220(2):1242–1259, 2020.
- [37] K. Xu and E. Darve. Spectral Method for the Fractional Laplacian in 2D and 3D. *arXiv e-prints*, page arXiv:1812.08325, Dec. 2018.

DEPARTMENT OF MATHEMATICAL SCIENCES AND THE CENTER FOR MATHEMATICS AND ARTIFICIAL INTELLIGENCE (CMAI), GEORGE MASON UNIVERSITY, FAIRFAX, VA 22030, USA.

Email address: hantil@gmu.edu

ABTEILUNG FÜR ANGEWANDTE MATHEMATIK, ALBERT-LUDWIGS-UNIVERSITÄT FREIBURG, HERMANN-HERDER-STRASSE 10, 79104 FREIBURG I. BR.

Email address: patrick.dondl@mathematik.uni-freiburg.de, ludwig.striet@mathematik.uni-freiburg.de